Soft Matter

ARTICLE TYPE

Cite this: DOI: 00.0000/xxxxxxxxxx

Symmetry- ased Classification of Forces Driving Chromatin Dynamics

Iraj Eshghi, lexandra Zidovska, lexander Y. Grosberg*

Received Date
Accepted Date

DOI: 00.0000/xxxxxxxxxx

Chromatin - the functional form of DN in the cell - exists in the form of a polymer immersed in a nucleoplasmic fluid inside the cell nucleus. Both chromatin and nucleoplasm are subject to active forces resulting from local biological processes. This activity leads to non-equilibrium phenomena, affecting chromatin organization and dynamics, yet the underlying physics is far from understood. Here, we expand upon a previously developed two-fluid model of chromatin and nucleoplasm by considering three types of activity in the form of force dipoles – two with both forces of the dipole acting on the same fluid (either polymer or nucleoplasm) and a third, with two forces pushing chromatin and solvent in opposite directions. We find that this latter type results in the most significant flows, dominating over most length scales of interest. Due to the friction between the fluids and their viscosity, we observe emergent screening length scales in the active flows of this system. We predict that the presence of different activity types and their relative strengths can be inferred from observing the power spectra of hydrodynamic fluctuations in the chromatin and the nucleoplasm.

1 Introduction

The genome resides inside the eukaryotic cell nucleus, and carries the information needed for the cell's life[1]. The nuclear interior is filled with nucleoplasm, the solvent, within which the genome is tightly packed: 2 meters of DNA in a nucleus about 10 microns in diameter[2]. In this state, the genome takes on a polymeric form composed of DNA and associated proteins, known as chromatin[3]. Chromatin is subject to a variety of ATP-dependent active processes such as transcription, replication and DNA repair[4]. This activity therefore affects chromatin's motions and organization[5].

The dynamics of chromatin were initially measured through the tracking of specific genomic structures such as telomeres[6] or single genes[7–9]. The single-gene studies found that chromatin moved in a constrained, subdiffusive manner at short times, but occasionally exhibited directed motion on longer time scales[7–9]. More recently, the development of Displacement Correlation Spectroscopy (DCS) has allowed for simultaneous nucleus-wide measurements of chromatin dynamics[10]. DCS uncovered that chromatin displays two regimes of motion: fast, uncorrelated motion at short times, and slow correlated motion at long times. The long-time motion is coherent on scales of about 3 5 μm[10]. These correlations disappear upon the depletion of ATP, as well as inhibition of nuclear enzymes such as RNA polymerase II, DNA polymerase and topoisomerase II, while being unaffected by cytoskeletal perturbations[10,11]. This demonstrates that enzymes in the cell nucleus produce coherent motion of chromatin.

Motivated by the DCS measurements, the first theory of active chromatin hydrodynamics was developed[12]. This study introduced two types of events, scalar and vector, and identified the vector events as those driving the large-wavelength fluctuations leading to micron-scale coherent motions observed in experiments[10]. It was soon followed by a numerical study, modeling chromatin as a coarse-grained polymer with hydrodynamic interactions, driven by active force dipoles[11]. This model investigates the hydrodynamics of the vector events. Specifically, it studies the effects of contractile and extensile dipoles, revealing that extensile dipolar forces are needed for large-scale chromatin motions to occur[11]. The main difference in approaches of these two works[11,12] is how the driving forces are modeled. In[12], each (vector) active source was presented as a force dipole with two equal and opposing forces acting on two locations in the polymer. In[11], one of the forces of the dipole was exerted on a polymer and the other on the solvent (albeit in the location point of the neighboring monomer). This seemingly subtle difference turned out to be very important: as we will show in this paper, the choice to organize the force dipoles in such a way leads to dramatic differences in the resulting active flows. On a more technical level, the numerical algorithm implemented in[11] treated hydrodynamics of the solvent under this point-like force in terms of a Stokeslet appropriately modified to meet the no-slip condition at the nuclear boundary. Such an approach chooses to

* *Center for Soft Matter Research, Department of Physics, New York University, New York, NY 10003, USA. E-mail: ayg1@nyu.edu*

neglect the hydrodynamic screening due to the polymer matrix.

Several hydrodynamics-free models of chromatin dynamics have been developed since then. A first group of them have focused on developing effective polymer models, homopolymers or heteropolymers, whose interaction parameters are extracted from experimental data of chromatin conformations from chromosome conformation capture (Hi-C) experiments[13]. These studies predicted the effect of confinement and tight packing on chromatin[14], reproduced experimental dynamical results such as coherent motion[15,16] and found glassy, heterogeneous dynamics in model chromosomes[16]. Such models have also reproduced general features of Hi-C contact maps and nuclear-scale chromosome architecture, such as reproducing contact probabilities from select chromosomes[17]. In contrast, other models consider chromatin as a simple chain with few free parameters, allowing for the study of the effects of athermal noise on chromosomal loci[18] or the effects of chromatin's fractal structure on its dynamics[19,20]. Simulations of such simple chains have allowed for studying the relationship between dynamics and the establishment of epigenetic domains[21]. Finally, continuum approaches have also been developed to model the process of phase separation of chromatin compartments in the nucleus[22], showing that much of the organization of chromatin can be accounted for by the process of liquid-liquid phase separation.

In this work, we seek to identify the minimal active ingredients needed to reproduce the ATP-dependent coherent motion of chromatin. To this end, we build upon an existing continuum, two-fluid model of chromatin dynamics which was introduced in[12]. A hydrodynamic framework is a natural approach for studying the motion of chromatin on length scales larger than the thickness of the polymer. While some earlier studies were able to reproduce coherent motions of chromatin without explicit accounting for hydrodynamics, those models rely on chromatin polymer conformations obtained by HiC.[15,23] These conformations are directly affected by hydrodynamics as they formed in the presence of the fluid (nucleoplasm) and fluid-mediated interactions in the cell nucleus *in vivo*. Our approach follows the study[11], which includes hydrodynamics explicitly and unambiguously: they model this system as a simple chain in a solvent with stochastically activated force dipoles, and obtain coherent motion of the polymer as a result.

The continuum approach allows for the inclusion of active events and hydrodynamic interactions of the polymer while remaining analytically tractable. A field-theoretic approach to studying the active behavior of chromatin allows us to explicitly harness the symmetries and conservation laws in this system, such as total conservation of solvent and chromatin. Activity can be included in a way that naturally respects such symmetries. Finally, the onset of collective behavior such as the emergence of coherent flows in chromatin[10] is easily studied with continuum frameworks, since the mathematical tools already developed in the study of phase transitions can be applied to this system as well.

We begin in Section II by describing the two-fluid model, which will serve as the basis for our description of the chromatin-nucleoplasm system. Then, we identify three possible types of active sources which can act on such a system in a momentum-conserving, localized way. The three types of active sources are distinguished in the way they couple to the two fluids. In Section III, we proceed to calculate the expected hydrodynamic flows that isolated sources of each activity type would generate in our chromatin model. Finally, in Section IV, we use these single-source flows to calculate the expected power spectra of polymer and solvent fluctuations, assuming a uniform and uncorrelated distribution of active events.

2 Three types of vector activity driving flows in chromatin

2.1 The model and equations of motion

Following previous work[12], we describe chromatin and its solvent, nucleoplasm, as a mixture of two fluids which dissipate energy when moving past one another. As in the previous work, we employ the equations of motion derived for such a polymer and solvent mixture by Doi and Onuki in[24]. In addition, we include two novel aspects with regard to the system's chromatin hydrodynamics[12], namely, we keep account of the solvent viscosity and we extend the application of the active body forces to both the polymer and the solvent. To write down the equations of motion for the two-fluid system, let the polymer (i.e., chromatin) velocity field be $\mathbf{v}^{\mathrm{p}}\ \mathbf{r})$ and its volume fraction $\phi\ \mathbf{r})$. The solvent velocity field is $\mathbf{v}^{\mathrm{s}}\ \mathbf{r})$, and its volume fraction $1\quad\phi\ \mathbf{r})$. The equations of motion are:

$$\begin{aligned}
\zeta\ \mathbf{v}^{\mathrm{p}}\quad\mathbf{v}^{\mathrm{s}}) &= \nabla\cdot\sigma\quad\nabla\Pi\quad\phi\nabla P+\ ^{\mathrm{p}}\\
\zeta\ \mathbf{v}^{\mathrm{s}}\quad\mathbf{v}^{\mathrm{p}}) &= \eta^{\mathrm{s}}\nabla^2\mathbf{v}^{\mathrm{s}}\quad 1\quad\phi)\nabla P+\ ^{\mathrm{s}}\\
\partial_t\phi &= \quad\nabla\cdot\ \phi\mathbf{v}^{\mathrm{p}}) = \nabla\cdot\quad 1\quad\phi)\,\mathbf{v}^{\mathrm{s}})
\end{aligned}\tag{1}$$

Here, ζ is a friction coefficient of polymer against solvent, per unit volume. Π,σ are the osmotic pressure and stress tensor of the polymer, respectively. Generally, σ is a function of $\mathbf{v}^{\mathrm{p}}$, the specific form of which depends on the type of fluid. For example, for a simple Newtonian fluid we have that $\nabla\cdot\sigma=\eta^{\mathrm{p}}\nabla^2\mathbf{v}^{\mathrm{p}}$, where η^{p} is polymer viscosity. Π is assumed to be an equilibrium function of density $\phi\ \mathbf{r})$ because it equilibrates quickly and locally, P is the hydrostatic pressure, and η^{s} is the viscosity of the solvent. In this paper, we include the latter in order to study the effects of hydrodynamic screening (as explained in Appendix A). Finally, $^{\mathrm{p,s}}$ are the force densities (forces per unit volume) acting on the polymer and solvent, respectively, $^{\mathrm{s}}$ being a new addition upon previous considerations to allow for a more complete description of possible forces. The arrangement of $^{\mathrm{p,s}}\ \mathbf{r},t)$ determines the activity-generated flows in the two-fluid model.

To highlight the main features of the proposed model, it is useful to juxtapose it with previous works[11,12], from which this work descends. These studies effectively consider different types of vector activity, with[12] considering vector events acting on the polymer only, while[11] considers events that act on the polymer and the solvent simultaneously, in opposite directions. In the present work, we will address the fact that upon considering both $^{\mathrm{p}}$

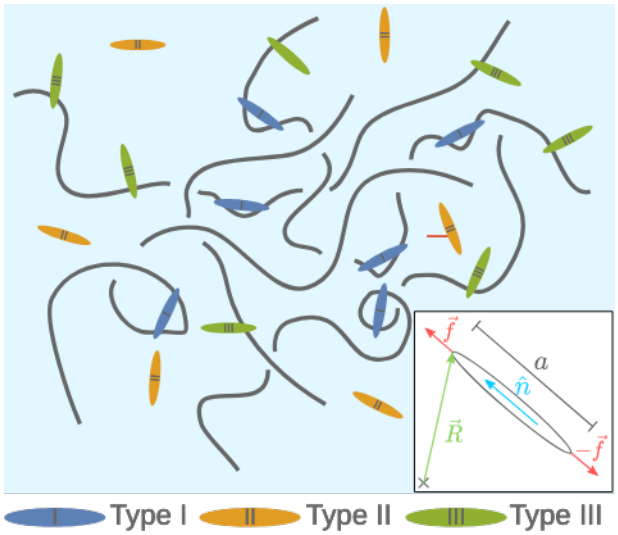

Fig. 1 artoon of the different types of activity considered, distinguished by whether they exert force on the polymer, the solvent, or both. Inset: Schematic representation of the geometry and force arrangement in a single vector source. a is the size of the motor, $\hat{\mathbf{n}}$ is a unit vector defining its orientation, $\mathbf{R}$ and $\mathbf{R}\ a\hat{\mathbf{n}}$ are centers where two forces $f\hat{\mathbf{n}}$ and $f\hat{\mathbf{n}}$ are exerted, forming a force dipole. The force dipole shown in the inset is extensile, while a contractile dipole would have the force vectors pointing inward instead of outward.

and ^{s}, there might be multiple types of vector sources which would couple differently to the two fluids, and we will generalize the field theoretic consideration of[12], accounting for events like the ones considered in[11]. In addition, we will consider explicitly the solvent viscosity to account for hydrodynamic screening. We therefore set out to expand the classification of possible active sources based on considerations of symmetry and conservation laws in the framework of the model described in Eqs. (1). We will focus on vector activity and not the scalar activity as identified in[12], since our new symmetry considerations do not add to the discussion on scalar events. Moreover, we show in Appendix B that there is a formal connection between scalar and vector events, where scalar events can be expressed as a superposition of vector events, and thus the latter can be considered as a sufficient basis for describing both types of activity.

2.2 Active forces generated by different types of motors

The arrangement of the forces in the system must obey both linear and angular momentum conservation. Active driving forces are produced by different types of motors. Without making any assumptions about their mechanism, we imagine a motor as a solid body of a size a (~ 10 nm^2) which is completely overdamped in the surrounding chromatin and nucleoplasm medium. As such, it can exert only balanced forces and torques on the fluid. In the simplest case, the resulting force distribution on the fluid must, on length scales larger than a, be that of a dipole (for a more detailed discussion on other activity types that could be included, see Appendix B).

Based on these conditions, we consider every source to be as a force dipole as shown in the inset of Fig. 1. They can be extensile (in the case $f > 0$) or contractile (if $f < 0$). It is also worth noting that in the overdamped scenario we consider here, the flows resulting from extensile or contractile sources are simply time-reversed versions of one another. Furthermore, all these driving motors have finite processivity. We imagine that they start at some random time and then their force decays proportional to some function $\kappa\ t)$ with time scale τ_f (further details regarding estimates for forces and time scales are shown in Appendix D), for instance $\kappa\ t) = e^{\ t/\tau_f}$. Three types of activity are then classified based on where their forces act: Type I, when both forces act on the polymer, Type II, when both forces act on the solvent, and Type III, when one force acts on each fluid.

2.2.1 Type I activity: both forces of the same dipole act on the polymer

The first possibility we consider is for the forces to be entirely exerted on the polymer. In this case, we approximate the force dipole generated by the motor as a pair of opposite forces exerted in points $\mathbf{R}$ and $\mathbf{R}\ a\hat{\mathbf{n}}$ (see Fig. 1, inset), such that the force density entering eq. (1) has the form

$$\begin{aligned} {}^{s}\ \mathbf{r}) &= 0 \\ {}^{p}\ \mathbf{r}) &= f\kappa\ t)\hat{\mathbf{n}}\ \delta\ \mathbf{r}\quad \mathbf{R})\quad \delta\ \mathbf{r}\quad \mathbf{R}+a\hat{\mathbf{n}})) \\ &\simeq\ af\kappa\ t)\hat{\mathbf{n}}\ \hat{\mathbf{n}}\cdot\nabla)\delta\ \mathbf{r}\quad \mathbf{R}), \end{aligned} \tag{2}$$

where the last transformation is justified by assuming that all relevant fields change only smoothly over the scale a. Here, f is a force magnitude. In previous work[12], this event was referred to as vector activity .

2.2.2 Type II activity: both forces of the same dipole act on the solvent

Type II activity is analogous to Type I, except that the dipoles exert their forces on the solvent. Thus, if the dipole points along $\hat{\mathbf{n}}$:

$$\begin{aligned} {}^{s}\ \mathbf{r}) &= f\kappa\ t)\hat{\mathbf{n}}\ \delta\ \mathbf{r}\quad \mathbf{R})\quad \delta\ \mathbf{r}\quad \mathbf{R}+a\hat{\mathbf{n}})) \\ &\simeq\ af\kappa\ t)\hat{\mathbf{n}}\ \hat{\mathbf{n}}\cdot\nabla)\delta\ \mathbf{r}\quad \mathbf{R}) \\ {}^{p}\ \mathbf{r}) &= 0 \end{aligned} \tag{3}$$

2.2.3 Type III activity: one force from the dipole acts on the polymer the other acts on the solvent

Finally, there is the possibility that a motor can exert a pair of equal forces in opposite directions, in the solvent and polymer, respectively. As a convention, we choose the orientation of the vector $\hat{\mathbf{n}}$ to point towards the polymer end of the dipole. Then, the forces are:

$$\begin{aligned} {}^{s}\ \mathbf{r}) &= \ \hat{\mathbf{n}}f\kappa\ t)\delta\ \mathbf{r}\quad \mathbf{R}+a\hat{\mathbf{n}}) \\ {}^{p}\ \mathbf{r}) &= \hat{\mathbf{n}}f\kappa\ t)\delta\ \mathbf{r}\quad \mathbf{R}) \end{aligned} \tag{4}$$

All types of activity exhibit the same form for the total force density $^{\rm p} + {}^{\rm s} \simeq af\hat{\mathbf{n}}\,\hat{\mathbf{n}}\cdot\nabla)\delta\ \mathbf{r} \quad \mathbf{R})$, which meets the momentum conservation condition.

3 Flows resulting from isolated events

3.1 Simplifications and approximations

For conceptual simplicity, in this section we consider the flows resulting from the action of a single active dipole. We evaluate this for all three types of active events we introduced in Section II. Further, we consider a linearized approximation, assuming that polymer density deviates only slightly from a spatially uniform value ϕ_0, namely $\phi\ r) = \phi_0 + \delta\phi\ r)$. Within this range, polymer osmotic pressure Π can be approximated as a linear function of density: $\Pi = \Pi_0 + K\delta\phi\ r)$ where K is the osmotic rigidity of the polymer matrix. Similarly, the polymer stress tensor is a linear function of velocities. For simplicity we assume that this dependence, just as that of osmotic pressure, is local in space, but it can have memory in time:

$$\nabla\cdot\sigma = \eta^{\rm p}\ t) * \ \nabla^2\mathbf{v}^{\rm p}), \tag{5}$$

where * means convolution with the time-dependent causal kernel $\eta^p\ t)$.

We also make the assumption of an infinite boundless domain. In that case, we can resort to Fourier transforms in both space and time, following standard convention

$$\begin{aligned} f\ \mathbf{r},t) &= \int \frac{d\omega d^3\mathbf{q}}{2\pi)^4} f_{\mathbf{q},\omega} e^{i\ \mathbf{q}\cdot\mathbf{r}\quad \omega t)} \\ f_{\mathbf{q}\omega} &= \int d^3\mathbf{r}dt f\ \mathbf{r},t) e^{\ i\ \mathbf{q}\cdot\mathbf{r}\quad \omega t)}, \end{aligned} \tag{6}$$

which allows a separate consideration of transverse (divergence-free) and longitudinal flows.

Finally, we introduce the ratio of the frequency-dependent viscosity of the polymer, and the constant viscosity of the solvent.

$$\chi_\omega = \eta^{\rm p}_\omega/\eta^{\rm s} \tag{7}$$

It is noteworthy that the time-dependent kernel $\eta^{\rm p}\ t)$ has units of viscosity per unit time, whereas $\eta^{\rm s}$ has units of viscosity. Thus, the ratio χ_ω is unitless, since Fourier transforming in time multiplies the units of $\eta^{\rm p}\ t)$ by time. If the polymer viscosity is constant, then $\eta^{\rm p}$ has units of viscosity, and χ is a unitless constant. For the frequencies of interest, χ_ω is much larger than 1, allowing us to simplify expressions below.

The physical effects left out from the framework of our simplified treatment include non-linear rheological response of the polymer, such as shear-thinning and/or -thickening effects. These effects would be important if the shear in the system is too large, which we do not expect to be the case in the real systems driven by molecular motors, which exert forces on the order of 10 pN[25] (more detailed estimates of the forcing from an example molecular motor can be found in Appendix D). Another group of neglected effects has to do with non-locality of rheological response (see[26]), which are expected to become important at sufficiently small length scales or long time scales. For measurement times of about a second, the non-local effects become significant when $r \ll 1\mu$m. In such a regime, the scaling of the resulting velocity profiles would be significantly affected (for more details on the estimation of this regime, see Appendix D). Since the value of a micron is close to the lengthscales we are interested in, these nonlocal rheology effects are likely significant to the problem we are studying. Nevertheless, we choose to neglect them at present, leaving their consideration for a later study. Our results would also be affected by the presence of boundaries, both in space and time. Finite time effects in this case should be negligible, because the time scales we are interested in are on the order of seconds whereas the interphase of a typical cell lasts for periods of over several hours[2]. Since the equations of motion we consider are linear, spatial boundaries can be dealt with by considering collections of image sources induced by the boundary conditions, in analogy with electrostatics.

3.2 Transverse flows

Transverse flows are those which are perpendicular to the wavevector $\mathbf{q}$ for a given Fourier mode. In real space the resulting fields are divergence-free, meaning they are not associated with any density variations. Indeed, applying the transverse projection operator to the linearized equations eliminates the field $\delta\phi$, and thus the variables of motion are only $\mathbf{v}^{\rm s}_\perp$ and $\mathbf{v}^{\rm p}_\perp$, where $\perp$ denotes the transverse component of a field. This results in the equations

$$\begin{aligned} \zeta\ \mathbf{v}^{\rm p}_\perp \quad \mathbf{v}^{\rm s}_\perp) &= \nabla\cdot\sigma_\perp + \ {}^{\rm p}_\perp \\ \zeta\ \mathbf{v}^{\rm s}_\perp \quad \mathbf{v}^{\rm p}_\perp) &= \eta^{\rm s}\nabla^2\mathbf{v}^{\rm s}_\perp + \ {}^{\rm s}_\perp, \end{aligned} \tag{8}$$

where $\nabla\cdot\sigma$ is given by Eq. (5). Notice that in the terms ${}^{\rm p}_\perp$, ${}^{\rm s}_\perp$ we are implicitly taking the transverse part of a source, which is singular, as shown in (2-4). This is a nontrivial matter which we discuss in Appendix C. The equations of motion (8) can be solved by Fourier transform in space and time (the ω dependence will be suppressed except where specifically relevant)

$$\begin{aligned} v^{\rm p}_{\perp\ \mathbf{q}} &= \frac{1}{\eta^{\rm p}}\left[H\ _{\beta\mathbf{q}}\left(F^{\rm p}_{\beta\mathbf{q}} + F^{\rm s}_{\beta\mathbf{q}}\right) + G\ _{\beta\mathbf{q}}F^{\rm p}_{\beta\mathbf{q}}\right] \\ v^{\rm s}_{\perp\ \mathbf{q}} &= \frac{1}{\eta^{\rm p}}\left[H\ _{\beta\mathbf{q}}\left(F^{\rm p}_{\beta\mathbf{q}} + F^{\rm s}_{\beta\mathbf{q}}\right) + \chi G\ _{\beta\mathbf{q}}F^{\rm s}_{\beta\mathbf{q}}\right], \end{aligned} \tag{9}$$

where the $\mathbf{q}$-dependent tensors $G\ _{\beta\mathbf{q}}$ and $H\ _{\beta\mathbf{q}}$ are defined as follows:

$$\begin{aligned} G\ _{\beta\mathbf{q}} &= \frac{\delta\ _{\beta} \quad q\ q_\beta)/q^2}{1/l^2 + q^2} \\ H\ _{\beta\mathbf{q}} &= \frac{\delta\ _{\beta} \quad q\ q_\beta)/q^2}{l^2q^2\ 1/l^2 + q^2)} \end{aligned} \tag{10}$$

In Eqs. (9-10), repeated indices are summed over, except for $\mathbf{q}$. We define $q = |\mathbf{q}|$, and $l = \sqrt{\eta^{\rm s}/\zeta}$. Note that the length scale l is of the order of the polymer mesh size, as it follows from the physical meaning of friction coefficient ζ. Inverting the Fourier

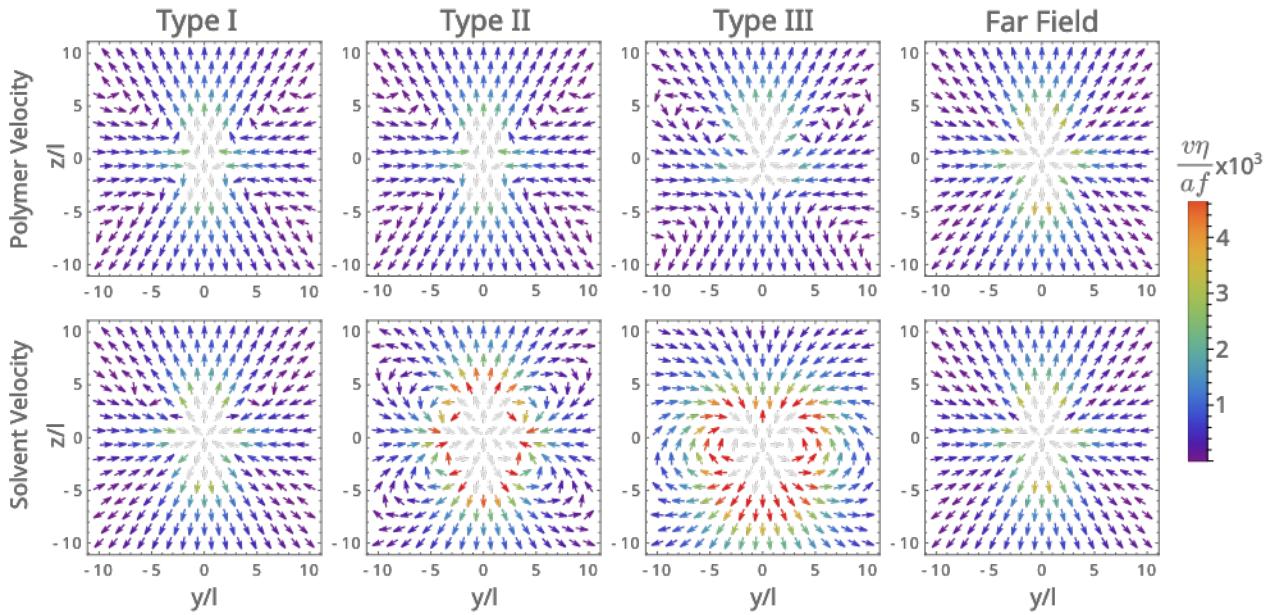

Fig. 2 Transverse flows showing yz components of vector fields in Eqs. (16)-(18), where $\hat{\mathbf{n}} = \hat{\mathbf{z}}$. $\mathbf{v}^{\mathrm{s}}$ is shown in the top row and $\mathbf{v}^{\mathrm{p}}$ on the bottom, for $\chi = 10$.

transform, one obtains in real space

$$G_{\alpha\beta}(r) = \frac{1}{4\pi r}\left(\delta_{\alpha\beta} h_1(r/l) + \frac{r_\alpha r_\beta}{r^2} h_2(r/l)\right)$$
$$H_{\alpha\beta}(r) = \delta_{\alpha\beta}(r) - G_{\alpha\beta}(r) \tag{11}$$
$$\delta_{\alpha\beta}(r) = \frac{1}{8\pi r}\left(\delta_{\alpha\beta} + \frac{r_\alpha r_\beta}{r^2}\right),$$

where auxiliary functions are defined below:

$$h_1(x) = x^2 + e^{-x}(1 + x^{-1} + x^{-2})$$
$$h_2(x) = 3x^{-2} - e^{-x}(1 + 3x^{-1} + 3x^{-2}) \tag{12}$$

We included in Eq. (10) the standard Oseen tensor (also called Stokeslet), which is just the Green's function of the usual low Reynolds number hydrodynamics[27].

Since the field theoretic framework of this paper is valid only on scales above the mesh size, we consider the above solutions, in Eq. (11) in the range $r \gg l$. For this example, we ignore the frequency dispersion of polymer viscosity (i.e., assuming $\chi_\omega = \chi$ constant):

$$G_{\alpha\beta}(r) \simeq \frac{l^2}{4\pi r^3}\left(3\frac{r_\alpha r_\beta}{r^2} - \delta_{\alpha\beta}\right) \tag{13a}$$

$$H_{\alpha\beta}(r) \simeq \delta_{\alpha\beta}(r) = \frac{1}{8\pi r}\left(\delta_{\alpha\beta} + \frac{r_\alpha r_\beta}{r^2}\right) \tag{13b}$$

To better understand the origin and meaning of these two tensors, we consider the dynamics of the field $\mathbf{w} = \mathbf{v}^{\mathrm{p}}_\perp - \mathbf{v}^{\mathrm{s}}_\perp$, describing the relative velocity of polymer and solvent. $\mathbf{w}$ obeys the following equations:

$$\zeta(1+\chi)\mathbf{w} - \eta^{\mathrm{p}}\nabla^2\mathbf{w} = -\nabla^{\mathrm{p}}_\perp - \chi\nabla^{\mathrm{s}}_\perp \tag{14}$$

The solution of this equation is directly obtained by subtracting Eqs. (9) from one another:

$$w_{\mathbf{q}} = \frac{1}{\eta^{\mathrm{p}}} G_{\alpha\beta\mathbf{q}}\left(F^{\mathrm{p}}_{\beta\mathbf{q}} - \chi F^{\mathrm{s}}_{\beta\mathbf{q}}\right) \tag{15}$$

This means that $G_{\alpha\beta\mathbf{q}}$ plays the role of Green's function for Eq. (14). In real space, $G_{\alpha\beta}(r)$ (13a) falls off at large distances as $1/r^3$, significantly faster than the regular Stokeslet (or Oseen tensor) in Eq. (13b); in Fourier space, of course, this corresponds to the factor $1/(l^{-2} + q^2)$. This is the phenomenon of hydrodynamic screening. Accordingly, Eq. (14) is referred to as the screened Stokes equation[28]. Thus, relative shear $\mathbf{w}$ of the solvent past polymer is suppressed beyond the distance l of the order of mesh size. Beyond this distance, polymer and solvent move largely together, which is why at these distances $H_{\alpha\beta}(r) \simeq O_{\alpha\beta}(r)$ (note that the latter comment is valid only for transverse components).

We now return to the velocity fields (9) resulting from the action of one dipole motor positioned in the origin. Plugging in the expressions of forces (2-4), we arrive at the following expressions for velocity fields driven by a single force dipole motor positioned at the origin:

Type I activity

$$v^{\mathrm{p}}_\perp(\mathbf{r}) = \frac{af\kappa(t)}{\eta^{\mathrm{p}}}\nabla_\gamma\left(H_{\alpha\beta} + G_{\alpha\beta}\right)\hat{n}_\beta\hat{n}_\gamma$$
$$v^{\mathrm{s}}_\perp(\mathbf{r}) = \frac{af\kappa(t)}{\eta^{\mathrm{p}}}\nabla_\gamma H_{\alpha\beta}\hat{n}_\beta\hat{n}_\gamma \tag{16}$$

	$l \ll r$	
Types I,II,III	$\mathbf{v}^{\mathrm{p}}_{\perp} \propto \frac{l^2}{r^2} P_2 \quad \cos\theta)\hat{\mathbf{r}}$ $\left(v^{\mathrm{p}}_{\perp}{}^2\right)_{\mathbf{q}} \propto \frac{\rho}{ql)^2} \ \lambda^2)_{\mathbf{q}}$	
Type I	$\mathbf{v}^{\mathrm{s}}_{\perp} \propto \frac{l^2}{r^2} P_2 \quad \cos\theta)\hat{\mathbf{r}}$ $\left(v^{\mathrm{s}}_{\perp}{}^2\right)_{\mathbf{q}} \propto \frac{\rho}{ql)^2} \ \lambda^2)_{\mathbf{q}}$	
Type II	$l \ll r \ll l\sqrt{\chi}$	$l\sqrt{\chi} \ll r$
	$\mathbf{v}^{\mathrm{s}}_{\perp} \propto \chi \frac{l^4}{r^4} \ P_1 \quad \cos\theta)\hat{\mathbf{n}} \quad P_2 \quad \cos\theta)\hat{\mathbf{r}})$ $\left(v^{\mathrm{s}}_{\perp}{}^2\right)_{\mathbf{q}} \propto \rho\chi^2 \ ql)^2 \ \lambda^2)_{\mathbf{q}}$	$\mathbf{v}^{\mathrm{s}}_{\perp} \propto \frac{l^2}{r^2} P_2 \quad \cos\theta)\hat{\mathbf{r}}$ $\left(v^{\mathrm{s}}_{\perp}{}^2\right)_{\mathbf{q}} \propto \frac{\rho}{ql)^2} \ \lambda^2)_{\mathbf{q}}$
Type III	$l \ll r \ll l^2\chi/a$	$l^2\chi/a \ll r$
	$\mathbf{v}^{\mathrm{s}}_{\perp} \propto \chi \frac{l^4}{ar^3} \ 3P_1 \quad \cos\theta)\hat{\mathbf{r}} \quad \hat{\mathbf{n}})$ $\left(v^{\mathrm{s}}_{\perp}{}^2\right)_{\mathbf{q}} \propto \rho\chi^2 \frac{l^2}{a^2} \ ql)^0 \ \mu^2)_{\mathbf{q}}$	$\mathbf{v}^{\mathrm{s}}_{\perp} \propto \frac{l^2}{r^2} P_2 \quad \cos\theta)\hat{\mathbf{r}}$ $\left(v^{\mathrm{s}}_{\perp}{}^2\right)_{\mathbf{q}} \propto \frac{\rho}{ql)^2} \ \lambda^2)_{\mathbf{q}}$

Table 1 Summary of leading behaviors for the velocity fields $\mathbf{v}^{\mathrm{s}}_{\perp}$, $\mathbf{v}^{\mathrm{p}}_{\perp}$ and their respective power spectra, as produced from the three source types in this study. The functions $\lambda^2)_{\mathbf{q}}$, $\mu^2)_{\mathbf{q}}$ are defined in Eq. (28). The different regimes are delineated by characteristic distances from the source, which correspond to the emergent screening lengths resulting from the friction and viscosity of the two fluids. The units of velocity in these expressions are $\frac{af}{\eta^{\mathrm{p}} l^2}$. Numerical factors are dropped along with the $\kappa \ t)$ time dependence. $P_n \ x)$ denotes the nth Legendre polynomial.

Type II activity

$$\begin{aligned} v^{\mathrm{p}}_{\perp} \quad \mathbf{r}) &= \quad \frac{af\kappa \ t)}{\eta^{\mathrm{p}}} \nabla_\gamma H \ _\beta \hat{n}_\beta \hat{n}_\gamma \\ v^{s}_{\perp} \quad \mathbf{r}) &= \quad \frac{af\kappa \ t)}{\eta^{\mathrm{p}}} \nabla_\gamma \ H \ _\beta + \chi G \ _\beta) \hat{n}_\beta \hat{n}_\gamma \end{aligned} \tag{17}$$

Type III activity

$$\begin{aligned} v^{\mathrm{p}}_{\perp} \quad \mathbf{r}) &= \frac{f\kappa \ t)}{\eta^{\mathrm{p}}} \ G \ _\beta \quad a\nabla_\gamma \ H \ _\beta) \hat{n}_\gamma) \hat{n}_\beta \\ v^{s}_{\perp} \quad \mathbf{r}) &= \quad \frac{f\kappa \ t)}{\eta^{\mathrm{p}}} \Big(\chi G \ _\beta + a\nabla_\gamma \ H \ _\beta + \chi G \ _\beta) \hat{n}_\gamma \Big) \hat{n}_\beta \end{aligned} \tag{18}$$

The above equations are written for simplicity neglecting the frequency dependence of polymer viscosity. In a more realistic case, when χ is a function of frequency, then in the above solutions all products $\kappa\chi$ turn into convolutions $\int \kappa \ t)\chi \ t \quad \tau) d\tau$. The spatial dependence remains unchanged.

Our intent is to describe flows at distances larger than the mesh size l, where our model is applicable. In the very far field, at $r \to \infty$, any one of the three activity types causes a similarly looking flow. This is because $H \sim r^{-1}$, while tensor G, describing the relative shear of solvent with respect to polymer, decays much faster, $G \sim r^{-3}$. That means these relative motions are screened out and irrelevant at sufficiently large distances, resulting in the flow field, in which polymer and solvent move together as

$$\begin{aligned} v^{s}_{\perp,} \quad \mathbf{r}) = v^{\mathrm{p}}_{\perp,} \quad \mathbf{r}) &= \quad \frac{af\kappa \ t)}{\eta^{\mathrm{p}}} \nabla_\gamma \quad _\beta \ \mathbf{r}) \hat{n}_\beta \hat{n}_\gamma \\ &= \frac{af\kappa \ t)}{\eta^{\mathrm{p}}} \frac{r}{8\pi r^3} \left(3 \ \cos^2\theta \quad 1 \right), \end{aligned} \tag{19}$$

where $\cos\theta = \hat{\mathbf{r}} \cdot \hat{\mathbf{n}}$. The flow field in Eq. (19) is exactly what we would expect from a force dipole af in an incompressible fluid medium. Although formula (19) is valid for any activity type, the range of distances where it is applicable changes between different types, as summarized in Table 1.

The flows generated by Type I activity belong to the long-range regime (19) for all $r \gg l$, since tensors G and H are multiplied by the same coefficient, and $G \sim H$ when $r \sim l$, and H decays far slower ($\sim r^{-1}$) than G does ($\sim r^{-3}$). For Type II, the shearing of polymer past solvent is enhanced by a factor of χ due to the source being in the solvent (see Eq. (14)). Therefore, a crossover in the resulting solvent flow takes place where $H \sim \chi G$, which is at a distance $r \sim l\sqrt{\chi}$. In contrast, Type III activity generates net transport of solvent and polymer past one another. In the flow equations, the resulting transition in regimes takes place when $\chi G \sim a\nabla H$, thus the onset of long-range behavior occurs at a larger distance: $r \sim \chi l^2/a$.

In all cases, the near-field flows of the polymer get screened on lengthscales larger than l due to the friction between the fluids, combined with the larger viscosity of the polymer relative to the solvent, and therefore v^{p} takes its long-range form for all length-scales in this model. The different scaling regimes for the behavior of the velocity fields are outlined in Table 1.

3.2.1 Extensile vs. contractile activity

It is worth asking the question of whether it makes a difference if these force dipoles are contractile or extensile. The calculations in this section are for extensile dipoles when $f > 0$. As mentioned earlier, there is a simple mapping which relates the two cases: if we take $f \to \quad f$ for our sources, then they become contractile. All of our flows are linear in f, so they simply switch sign. This can also be understood as a result of the reversibility of transverse low-Reynolds number hydrodynamics. Switching the sign of the source term in our equations is equivalent to running the system backwards in time, which implies all velocities switch sign.

3.3 Longitudinal flows

Due to the incompressibility of the system, the divergences of $\mathbf{v}^{\mathrm{p}}$, $\mathbf{v}^{\mathrm{s}}$ are both exactly described by $\delta\phi$, the local changes in the density of the polymer network. We denote the longitudinal components of the velocity and polymer flow fields $\mathbf{v}^{\mathrm{s}}_{\parallel}$, $\mathbf{v}^{\mathrm{p}}_{\parallel}$ respectively. Their dynamics are obtained by taking the divergence of Eq. (1). After applying continuity and incompressibility, we obtain

$$\begin{aligned}\left(1 \quad l^2\chi\nabla^2\right)\delta\dot{\phi} &= \frac{1 \quad \phi_0)^2}{\zeta/\phi_0}\nabla^2\Pi + F_0 \\ &\approx D\nabla^2\delta\phi + F_0\,,\end{aligned} \tag{20}$$

where $D = \frac{K\ 1 \quad \phi_0)^2}{\zeta/\phi_0}$ is the effective diffusion coefficient of the polymer. We have dropped a factor of $1 \quad \phi_0)^2$ multiplying the Laplacian on the left-hand-side for brevity, since ϕ_0 is expected to be of order $1/2$ and thus should not affect the magnitude significantly. F_0 is the following source term:

$$F_0 = \quad \frac{1 \quad \phi_0)^2}{\zeta/\phi_0}\nabla\cdot \quad \mathrm{p} \quad \frac{\phi_0}{1 \quad \phi_0} \quad \mathrm{s}) \tag{21}$$

The Laplacian acting on the time derivative makes this PDE difficult to evaluate, but on length scales larger than $l\sqrt{\chi}$ it reduces to a heat equation:

$$\delta\dot{\phi} = D\nabla^2\delta\phi + F_0\,, \tag{22}$$

Using the fact that $\mathbf{v}^{\mathrm{s}}_{\parallel}, \mathbf{v}^{\mathrm{p}}_{\parallel}$ are potential fields, we have (away from the singularity at the source):

$$\begin{aligned}\mathbf{v}^{\mathrm{s}}_{\parallel} &= \frac{D}{1 \quad \phi_0}\nabla\delta\phi \\ \mathbf{v}^{\mathrm{p}}_{\parallel} &= \quad \frac{D}{\phi_0}\nabla\delta\phi\end{aligned} \tag{23}$$

The solution to Eq. (22) can be found by convolution of the source with the fundamental solution to the heat equation in 3D, which in the absence of boundaries is known to be a Gaussian function, whose width increases as the square root of time.

As before, we can ask what happens if we take the sources to be contractile instead of extensile. In this case, performing the transformation $f \to \quad f$ flips the sign of the source term F_0, but does not qualitatively change the dynamics significantly. However, the dynamics are not reversible since diffusion plays a role, so we cannot simply map the contractile case to the time-reversed extensile case as we did for the transverse flows.

4 Flows resulting from ensembles of active events

In this section, we consider the flows generated by many motors of a single type. To this end, we will now consider an ensemble of events uniformly distributed in space and time in a system of infinite volume. We assume this ensemble to have a finite space-time density ρ. i.e. $\rho\ t\ v$ motors working simultaneously in a volume element v during a time interval t. We imagine these active sources to be randomly distributed in space and time. Thus, the resulting random velocity fields will be considered statistically and we will calculate the moments of their distribution.

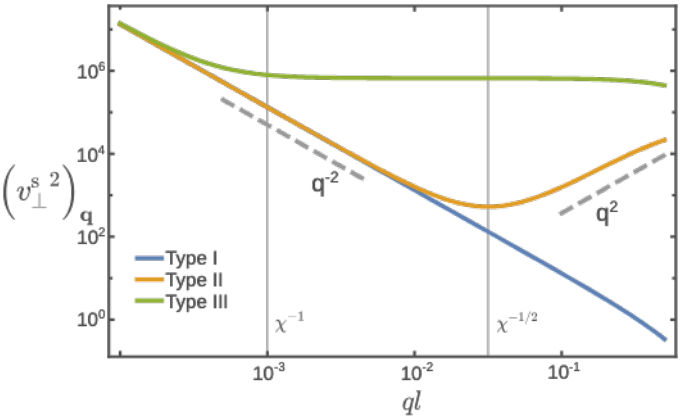

Fig. 3 Power spectra of transverse solvent fluctuations for three activity types (Type I, II and III), where velocity units are $\frac{af}{\eta^{\mathrm{p}}l^2}$, $\rho = 1$, $a = l$, and $\chi = 10^3$.

Each of the active sources turns on randomly at a time, and stays active for a period of time as described by the earlier defined function $\kappa\ t)$. We examine the orientation distribution of these events for a possible spatial order. Such orientation ordering would be different for different types of activity. Specifically, type III events are polar (since their two ends are different), and therefore may exhibit polar order with a non-zero average direction vector: $\langle\hat{\mathbf{n}}\rangle = \mathbf{M}$. By contrast, Type I and II motors are apolar, for them $\hat{\mathbf{n}}$ and $\quad\hat{\mathbf{n}}$ are physically equivalent, such that $\langle\hat{\mathbf{n}}\rangle = 0$. Accordingly, for them, orientation order is characterized by the nematic order parameter:

$$\langle\hat{n}\ \ \hat{n}_\beta\rangle = Q\ \ _\beta + \frac{1}{3}\delta\ \ _\beta\,, \tag{24}$$

Since we assume the system to be translationally invariant, the coarse-grained fields $Q\ \ _\beta$ and $M\ \ $ can be considered constant throughout the space.

In a spatially uniform system, average velocities must be zero, as it is clear from Eqs. (9) and (20) for transverse and longitudinal parts, respectively. Therefore, we will consider the power spectra of transverse and longitudinal velocity fluctuations, which are related to the second moments of the corresponding velocities distributions. As a reminder, the power spectrum of any field $s\ \mathbf{r},t)$, which we denote as $s^2)_{\mathbf{q}\omega}$ is defined by the relation

$$\langle s_{\mathbf{q}\omega}s^*_{\mathbf{q}'\omega'}\rangle = \quad t\quad v\left(s^2\right)_{\mathbf{q}\omega}\delta_{\mathbf{q}\mathbf{q}'}\delta_{\omega\omega'}\,, \tag{25}$$

where $s^2)_{\mathbf{q}\omega}$ is also the Fourier transform of the real-space correlation function $\langle s\ \mathbf{r},t)s\ 0,0)\rangle$.

4.1 Power spectrum of transverse fluctuations

The flows resulting from a single source at the origin, as described in Eqs. (16-18), are linear response relations. As such, the power spectra resulting from a uniform distribution of sources can be calculated in Fourier space by taking the squared magnitude of

the response function and multiplying it by the power spectrum of the source. In other words, for a general field $s_{\mathbf{q}\omega}$ obeying the following linear response relation with some response function $\mathscr{R}$ and a stochastic source f

$$s_{\mathbf{q}\omega} = \mathscr{R}_{\mathbf{q}\omega} f_{\mathbf{q}\omega} \tag{26}$$

we can obtain its power spectrum:

$$\left(s^2\right)_{\mathbf{q}\omega} = \left|\mathscr{R}^2\right|_{\mathbf{q}\omega} \left(f^2\right)_{\mathbf{q}\omega} \tag{27}$$

In our case, the tensorial structure of the response functions will only enter into the final power spectrum in the form of a transverse projection operator $\mathscr{P}_{\alpha\beta\mathbf{q}} = \delta_{\alpha\beta} - \frac{q_\alpha q_\beta}{q^2}$ acting on the source term. This results in two possible spectra, depending on whether the response function is linear in $\hat{\mathbf{n}}$ or has higher order dependence.

$$\begin{aligned} \lambda^2)_{\mathbf{q}} &= \langle \hat{q}_\alpha \hat{q}_\beta \hat{n}_\alpha \hat{n}_\beta \mathscr{P}_{\gamma\delta} \hat{n}_\gamma \hat{n}_\delta \rangle \\ &= \langle (\hat{\mathbf{q}}\cdot\hat{\mathbf{n}})^2 - (\hat{\mathbf{q}}\cdot\hat{\mathbf{n}})^4 \rangle \\ \left(\mu^2\right)_{\mathbf{q}} &= \langle \hat{n}_\alpha \mathscr{P}_{\alpha\beta} \hat{n}_\beta \rangle \\ &= 1 - \langle (\hat{\mathbf{q}}\cdot\hat{\mathbf{n}})^2 \rangle \end{aligned} \tag{28}$$

It is worth noting that in the case of an isotropic distribution of $\hat{\mathbf{n}}$, we have $\langle (\hat{\mathbf{q}}\cdot\hat{\mathbf{n}})^2 \rangle = 1/3$, $\langle (\hat{\mathbf{q}}\cdot\hat{\mathbf{n}})^4 \rangle = 1/5$. The tensors H and G can be rewritten by factoring out from them the transverse projection operator $\mathscr{P}_{\alpha\beta}$. Then, $H_{\alpha\beta\mathbf{q}} = h_q \mathscr{P}_{\alpha\beta\mathbf{q}}$ and $G_{\alpha\beta\mathbf{q}} = g_q \mathscr{P}_{\alpha\beta\mathbf{q}}$. Using the definitions in Eqs. (10), we obtain an expression for h_q, g_q:

$$\begin{aligned} g_q &= \frac{1}{1/l^2 + q^2} \\ h_q &= \frac{1}{l^2 q^2 (1/l^2 + q^2)} \end{aligned} \tag{29}$$

We then write down the power spectra for the polymer and solvent fluctuations resulting from all three source types.

Type I activity

$$\begin{aligned} \left(v_\perp^{\mathrm{p}\,2}\right)_{\mathbf{q}\omega} &= \left|\frac{af\kappa_\omega}{\eta_\omega^{\mathrm{p}}}\right|^2 \rho q^2 (h_q + g_q)^2 \lambda^2)_{\mathbf{q}} \\ \left(v_\perp^{\mathrm{s}\,2}\right)_{\mathbf{q}\omega} &= \left|\frac{af\kappa_\omega}{\eta_\omega^{\mathrm{p}}}\right|^2 \rho q^2 h_q^2 \lambda^2)_{\mathbf{q}} \end{aligned} \tag{30}$$

Type II activity

$$\begin{aligned} \left(v_\perp^{\mathrm{p}\,2}\right)_{\mathbf{q}\omega} &= \left|\frac{af\kappa_\omega}{\eta_\omega^{\mathrm{p}}}\right|^2 \rho q^2 h_q^2 \lambda^2)_{\mathbf{q}} \\ \left(v_\perp^{\mathrm{s}\,2}\right)_{\mathbf{q}\omega} &= \left|\frac{af\kappa_\omega}{\eta_\omega^{\mathrm{p}}}\right|^2 \rho q^2 (h_q + \chi_\omega g_q)^2 \lambda^2)_{\mathbf{q}} \end{aligned} \tag{31}$$

Type III activity

$$\begin{aligned} \left(v_\perp^{\mathrm{p}\,2}\right)_{\mathbf{q}\omega} &= \left|\frac{f\kappa_\omega}{\eta_\omega^{\mathrm{p}}}\right|^2 \rho \left[g_q^2 \mu^2)_{\mathbf{q}} + a^2 q^2 h_q^2 \lambda^2)_{\mathbf{q}}\right] \\ \left(v_\perp^{\mathrm{s}\,2}\right)_{\mathbf{q}\omega} &= \left|\frac{f\kappa_\omega}{\eta_\omega^{\mathrm{p}}}\right|^2 \rho [\chi_\omega^2 g_q^2 \mu^2)_{\mathbf{q}} \\ &\quad + a^2 q^2 (h_q + \chi_\omega g_q)^2 \lambda^2)_{\mathbf{q}}] \end{aligned} \tag{32}$$

It is important to note that the mean transverse flow of polymer and solvent is 0 in the isotropic case: upon taking an ensemble average of the Eqs. (16-18) with $\langle \hat{\mathbf{n}} \rangle = 0$ and the second moment defined as in (24), then the flows are all directly proportional to $Q_{\alpha\beta}$, and thus go to 0 in the isotropic limit. However, the second moment of the velocity distribution remains nonzero since in the isotropic case $\lambda^2)_{\mathbf{q}}$, $\mu^2)_{\mathbf{q}}$ remain nonzero. Importantly, the same power spectrum scaling is shared for all three types of activity in the solvent in the far field.

In the near field, the different scaling regimes for the power spectra are delineated by the screening length scales, which controlled the regimes for the Green's functions in Section III. Analogously to those results, we find that the power spectrum for polymer fluctuations is the same for all types of activity, and scales uniformly as q^{-2} for all length scales of interest, i.e., for $r \gg l$. In the far field, the solvent power spectrum follows the same scaling. However, scaling laws for velocity fluctuations change and cross over at the length scales $l\sqrt{\chi}$ and $l^2\chi/a$.

It is possible that two or all three types of activity may operate in the same system. In such a case, it is important to consider how their spectral signatures contribute to the total power spectrum of velocity fluctuations. If all types of activity are present in comparable amounts and with comparable power, Type III activity dominates the power spectrum of the solvent fluctuations across all length scales, with a transition from q^{-2} to q^0 behavior at the characteristic spatial frequency $q \sim (l^2\chi/a)^{-1}$. If Type III dipoles are absent, weak, or present in far smaller quantities than Types I and II, then the power spectrum of the solvent is dominated by Type II activity, with a transition from q^{-2} to q^2 dependence at around $q \sim (l\sqrt{\chi})^{-1}$. The polymer power spectrum is monotonous over the frequencies q of interest, scaling as q^{-2} with the prefactor characterizing an overall power scale $\left(\frac{af\kappa_\omega}{\eta_\omega^{\mathrm{p}}}\right)^2 \rho$.

The power spectra, being proportional to f^2, are unaffected by whether we choose the sources to be contractile or extensile. This remains true as long as the individual dipoles are non-interacting.

4.2 Power spectrum of longitudinal fluctuations

As in the case of longitudinal flows from a single source, the longitudinal power spectra of both $\mathbf{v}_\parallel^s$, $\mathbf{v}_\parallel^p$ will be determined from the fluctuation spectrum of $\delta\phi$, due to incompressibility:

$$\begin{aligned} \left(v_\parallel^{\mathrm{p}\,2}\right)_{\mathbf{q}} &= \frac{\omega^2}{q^2\phi_0^2} \left(\delta\phi^2\right)_{\mathbf{q}\omega} \\ \left(v_\parallel^{\mathrm{s}\,2}\right)_{\mathbf{q}} &= \frac{\omega^2}{q^2 (1 - \phi_0)^2} \left(\delta\phi^2\right)_{\mathbf{q}\omega} \end{aligned} \tag{33}$$

Since Eq. (20) is linear, the spectrum of density fluctuations is readily obtained:

$$\delta\phi^2)_{\mathbf{q}\omega} = \frac{F_0^2)_{\mathbf{q}\omega}}{|i\omega\ 1+\chi_\omega l^2 q^2)\quad Dq^2|^2} \tag{34}$$

The power spectra of the Type I and II sources are very similar to one another, but since Type III sources pull apart the two fluids in opposite directions, they have a more pronounced effect on the longitudinal dynamics. Similarly to before, the angular distribution of sources determines the quantities $\Gamma^2)_q$ and $\Omega^2)_q$:

$$\begin{aligned}\left(\Gamma^2\right)_{\mathbf{q}} &= \langle\ \hat{\mathbf{q}}\cdot\hat{\mathbf{n}})^4\rangle \\ \left(\Omega^2\right)_{\mathbf{q}} &= \langle\ \hat{\mathbf{q}}\cdot\hat{\mathbf{n}})^2\rangle\end{aligned} \tag{35}$$

Equipped with these expressions, we write the longitudinal power spectra for all three source types:

Type I activity

$$F_0^2)_{\mathbf{q}\omega} = |\nu_\omega|^2\ 1\quad \phi_0)^2 q^4 \left(\Gamma^2\right)_{\mathbf{q}} \tag{36}$$

Type II activity

$$F_0^2)_{\mathbf{q}\omega} = |\nu_\omega|^2 q^4 \left(\Gamma^2\right)_{\mathbf{q}} \tag{37}$$

Type III activity

$$\begin{aligned}F_0^2)_{\mathbf{q}\omega} &= \frac{|\nu_\omega|^2}{a^2} q^2 \left(\ aq)^2 \left(\Gamma^2\right)_{\mathbf{q}} + \left(\Omega^2\right)_{\mathbf{q}}\right) \\ &\simeq \frac{|\nu_\omega|^2}{a^2} q^2 \left(\Omega^2\right)_{\mathbf{q}},\quad q\ ^1 \gg a\end{aligned} \tag{38}$$

Here, we have defined $|\nu|^2_\omega = \rho\left|\frac{af\kappa_\omega}{\zeta}\right|^2\ 1\quad \phi_0)^2\phi_0^2$. It is clear that the longitudinal spectrum resulting from Type I and II activity is identical up to a factor of $1\quad \phi_0)^2$. Evidently, those two types of activity do not affect the density distribution in very contrasting ways. However, the third type of activity is dominated by a q^2 dependence for all length scales of interest (since we assume that a and l are both smaller than the coarse-graining scale of this theory). This is simply due to the fact that these types of sources shear the two fluids apart, and thus result in a much stronger spectrum of density fluctuations at long range (small q), compared to their counterparts.

Finally, just like in the transverse case, the longitudinal flow power spectra are unaffected by the contractile or extensile nature of the sources generating them.

5 Discussion

In this work, we have developed a classification scheme for the active forces that could act on a two-fluid system such as chromatin. We enforce conservation of linear and angular momentum, and know that the long-range effects of a force distribution are dominated by its lowest order multipole. Thus, we find that the dominant contribution to the flows comes from force dipoles. These force dipoles can then be of three different types, depending on which fluid each end acts upon. We have shown the effects of these three types of vector activity acting in a chromatin-nucleoplasm system: pairs of forces acting either both on the polymer (*Type I*), or both on the solvent (*Type II*), or one on the polymer and the other on the solvent (*Type III*). Their effects on the two fluids can be read out through the following dynamical fields: the solvent flow velocity field $\mathbf{v}^{\mathrm{s}}$, the polymer flow velocity field $\mathbf{v}^{\mathrm{p}}$, and the polymer density field ϕ.

We find that the flows generated by single active dipoles, and the power spectra resulting from collections of active events, do not change significantly if we consider contractile instead of extensile dipoles. This remains true as long as one neglects hydrodynamic interactions between the active bodies generating the force dipoles. As soon as such interactions are relevant, the difference between extensile and contractile dipoles becomes very significant, as was emphasized in [11].

We found that the friction between the two fluids in our model leads to hydrodynamic screening in the flows resulting from active sources. Two length scales are produced by this screening, dictated by the mesh size of the polymer $l = \sqrt{\frac{\eta^s}{\zeta}}$ and the (generally frequency-dependent) ratio between the viscosities of polymer and solvent, χ_ω. The different types of activity generate different magnitudes of flows, which leads to screening occurring on different scales. Specifically, Type III activity does not conserve momentum in any one fluid, since it pushes both fluids in opposite directions, thus it results in the largest screening length scale. Type I and II activity, in contrast, act only on one of the two fluids and conserve momentum within that fluid. Thus, the flows they generate in the solvent are screened within a smaller range from the source. Type II activity, since it acts on the solvent directly and the solvent has lower viscosity than the polymer, leads to a larger screening length than Type I activity, which is screened on the scale of the polymer mesh size. On length scales above these screening lengths, the polymer and solvent flow together in a pattern identical to a Stokeslet.

It is important to estimate what these screening lengths are, so that we may compare them to the known dimensions in the case of chromatin and nucleoplasm in a cell nucleus. We expect the mesh size, l, to range from around 30 nm to 100 nm [29,30]. The size of individual molecular motors, a, is on the order of 10 nm (the size of bacterial RNA polymerase has been measured to be 17 nm [31], and eukaryotic RNA polymerase II is around the same molecular weight [2]). In contrast, the ratio of viscosities χ is harder to estimate. Bare nucleoplasm has been measured to have a viscosity on the same order to that of water [32,33], $\eta^s \simeq 10^{\ 3}$ Pas , whereas a wide range of chromatin viscosities have been measured, $\eta^{\mathrm{p}} \approx 0\ 6\quad 3000$ Pas [34–39]. Thus, experimental ranges for

χ lie between 10^2 and 10^6. The two screening length scales we expect above the mesh size are $l\sqrt{\chi}$ and $l^2\chi/a$. At the upper limit of the estimates, these length scales become much larger than the size of the nucleus, making them irrelevant for our system of interest. The lower limits for their estimates are $l\sqrt{\chi} \approx 300$ nm and $l^2\chi/a \approx 4$ μm. For comparison, the size of the coherent domains in chromatin was found to be around 3 μm [10]. Therefore, there is a range of parameters consistent with existing experiments, which makes the screening lengths be comparable to the length scales which are relevant to chromatin's active dynamics as measured by DCS [10].

We calculated the power spectra for both active transverse and longitudinal fluctuations of the medium and found characteristic changes in the scaling of the power spectrum. The length scales at which these changes in scaling occur correspond to the screening length scales $l\sqrt{\chi}$ and $l^2\chi/a$ estimated above. Thus, from the spatial frequency dependence of the power spectra, parameters describing the material and its active components may be measured. For example, if the two length scales $l^2\chi/a$, $l\sqrt{\chi}$ were measured, with the prior knowledge of the motor size a, both the mesh size and the viscosity ratio of the chromatin-nucleoplasm system can be determined. By measuring the overall magnitude of the power spectrum itself, the quantity $\left(\frac{af}{\eta^{\mathrm{p}}}\right)^2 \rho$ can be measured. Given a and η^{p} (the latter is already measurable by looking at the screening length scales), this can be used to constrain the value of $f^2\rho$, which gives an estimate of the force density being injected into the system by active dipoles. Using values found in the literature, we can derive an estimate of $\left(\frac{af}{\eta^{\mathrm{p}}}\right)^2 \rho \approx 1$ $\mu\mathrm{m}^3\mathrm{s}^{-2}$ (for more details, see Appendix D).

Previous studies have focused on the power spectrum obtained from fluorescently-labeled chromatin [12]. This was used to identify the regimes of relevance for transverse and longitudinal fluctuations respectively, as seen in the polymer fluctuation spectrum. Here we have shown that additional information may be obtained by measuring the power spectrum of solvent fluctuations. In identifying the regimes in the power spectrum scaling (or lack thereof), it is possible to rule out types of activity present in the nucleoplasm (for example, if a q^0 scaling is absent, then Type III activity is either absent or present only in very small amounts), as well as measure the screening lengths in the two-fluid solution.

Thus, our description of transverse fluctuations takes few experimentally measurable parameters as inputs: the mesh size of chromatin, and the viscosities of chromatin and nucleoplasm. The model predicts that each type of source produces a particular q-dependence in the solvent velocity power spectrum, as outlined in Table 1. The values of the mesh size and viscosities give the length scales bounding different scaling regimes of q-dependence, as shown in Figure 3. These predictions may be be verified by future experiments. So far, the power spectrum of chromatin velocity fluctuations has successfully been measured using DCS [12]. A similar measurement for nucleoplasm dynamics, which would enable comparison with our predictions, has not been performed so far. Future experiments revealing the scaling exponents of the nucleoplasmic velocity power spectra and screening length scales delineating the crossovers may test our predictions.

6 Conclusions

We have extended a framework for the classification of active forces in a polymer-solvent system as a model for chromatin and nucleoplasm's active fluctuations. These active sources are approximated as first order in a multipole expansion, and classified based on the type of coupling they have to the two fluids, yielding three different categories of forces, each of which we found to generate a different scaling in power spectrum of solvent fluctuations. We considered these sources as independent and immovable. Yet, in the cell these motors could work cooperatively, hence the collective behavior of these sources is of much interest, as the motors which are the sources of the flows should be advected by chromatin and nucleoplasm themselves. Therefore, the consideration of the continuum dynamics of other fields, such as the density and orientation of these sources, will inform on the system's dynamics, including self-organization and alignment of the sources. In addition, consideration of the nuclear boundary may provide further insights into the active behavior of the system found *in vivo*.

Our model aims to study the genome's dynamical properties, by identifying and classifying the effects of different active sources on chromatin. This expands our understanding of the genome as a nonequilibrium system. It also contributes to our efforts to elucidate the physics of nonequilibrium materials by enriching the types of possible activity. Our symmetry-based classification scheme applies to any active system composed of two fluids, and could systematically be extended to multicomponent systems as well. For example, this framework could be extended to account for more components within the nucleoplasm which may interact preferentially with different forms of activity, or be extended to multiphase separated systems such as nucleoli [40,41]. Thus, we have shown that because of symmetry and conservation laws, there are few possible forms that active events can take in a two-fluid system. Then, it is straightforward to study the effects of these forces on the system of interest. In a complex biological system such as chromatin, with a myriad of different components interacting, this approach gives promising avenues for identifying and studying the possible sources for observed nonequilibrium effects.

uthor Contributions

A.Y.G. and A.Z. designed the project, I.E. and A.Y.G. performed calculations, A.Y.G., I.E. and A.Z. analyzed the data and wrote the paper.

Conflicts of interest

The authors declare no competing interests.

cknowledgements

A.Z. is grateful for support from the NSF Grants CAREER PHY-1554880, CMMI-1762506 and NYU MRSEC DMR-1420073. This research was supported in part by the National Science Foundation under Grant No. NSF PHY-1748958. A.Z. and A.Y.G. acknowledge useful discussions with participants of the 2020 virtual KITP program on Biological Physics of Chromosomes .

ppendix Solvent viscosity

The equations of motion presented in[12] are adequate for the description of fluids, where the viscosity of the solvent is a lot larger than that of the polymer (chromatin) but the resulting phenomenology does not capture the effects of hydrodynamic screening.

Here, we show with a simple argument, why this is the case. Consider the polymer to be a Newtonian fluid, such that $\nabla\cdot\sigma = \eta^{\rm p}\nabla^2\mathbf{v}^{\rm p}$. Then, consider the case, where the system is translationally symmetric in the x and y directions, so all dynamical parameters are only functions of z. Then, we have the following equations of motion:

$$\begin{aligned}\zeta\ \mathbf{v}^{\rm p}\quad\mathbf{v}^{\rm s}) &= \eta^{\rm p}\partial_z^2\mathbf{v}^{\rm p}\quad\hat{\mathbf{z}}\partial_z\Pi\quad\hat{\mathbf{z}}\phi_0\partial_z P\\ \zeta\ \mathbf{v}^{\rm s}\quad\mathbf{v}^{\rm p}) &= \quad\hat{\mathbf{z}}\ 1\quad\phi_0)\partial_z P\end{aligned}\tag{A39}$$

Now, consider a situation, where the half-space $z<0$ is filled with a polymer-solvent mixture, where the polymer is held fixed, so $\mathbf{v}^{\rm p}=0$. In the half-space $z>0$, we have $\phi=0$, and we impose a shear flow of solvent at a velocity $\mathbf{v}^{\rm s}=u\hat{\mathbf{x}}$.

The classical result for a colloidal solution in such an arrangement with a solvent of viscosity $\eta^{\rm s}$ is a screening effect where the solvent velocity goes $\mathbf{v}^{\rm s}\propto\hat{\mathbf{x}}e^{z/l}$ for $z<0$, with $l\sim\sqrt{\frac{\eta_s}{\zeta\phi_0}}$ where η_s is the solvent viscosity[42]. Such a screening cannot result from Eqs. (39). Since $\mathbf{v}^{\rm s}\quad\mathbf{v}^{\rm p}\propto\hat{\mathbf{z}}\partial_z P$, no difference in flow is possible along the shear direction $\hat{\mathbf{x}}$. This means that no friction along that direction is permissible, and thus no screening.

This is remedied by the addition of a stress tensor for the solvent, which in our case we take to be Newtonian. Thus, we add a term $\eta^{\rm s}\nabla^2\mathbf{v}^{\rm s}$ to the second equation of motion. We then obtain

$$\begin{aligned}\zeta\ \mathbf{v}^{\rm p}\quad\mathbf{v}^{\rm s}) &= \eta^{\rm p}\nabla^2\mathbf{v}^{\rm p}\quad\nabla\Pi\quad\phi_0\nabla P\\ \zeta\ \mathbf{v}^{\rm s}\quad\mathbf{v}^{\rm p}) &= \eta^{\rm s}\nabla^2\mathbf{v}^{\rm s}\quad 1\quad\phi_0)\nabla P\end{aligned}\tag{A40}$$

which, in the 1D shear situation presented above, allows a solution $\mathbf{v}^{\rm s}\propto\hat{\mathbf{x}}e^{z/l}$ for $z<0$ with $l=\sqrt{\frac{\eta_s\chi}{\zeta\ 1+\chi)}}$, where χ is the ratio of viscosities $\eta^{\rm p}/\eta^{\rm s}$.

ppendix B Higher multipole moments

Our consideration is based on force dipoles. One may ask if higher order force multipoles can be relevant. In general, we can perform a multipole expansion of our system's force distribution. For the $n^{\rm th}$ order of the expansion, the responding flows will decay like $r^{\ n+1)}$. By momentum conservation we expect the monopole $n=0$) term to be 0, and then terms higher than the dipole will be sub-dominant in the far field. Since the length scales we are considering are larger than the motors themselves, the far-field expansion applies here. Furthermore, the torque-free condition means pairs of forces must act along a single line. Therefore, the local building blocks of the force distribution must be force dipoles of the three types outlined in the main text.

In the formal structure of our theory, it is worth noting that there exists a (purely mathematical) correspondence between scalar active events and a certain arrangement of dipolar sources. First of all, notice that any shift in osmotic pressure in one of the fluids is equivalent to an opposite shift in the second fluid's osmotic pressure, up to a scale factor. This is a consequence of incompressibility: the chemical potential of this system is an *exchange* chemical potential. Formally speaking, adding any pressure $\nabla\pi$ in the polymer is equivalent to a pressure $\frac{1-\phi_0}{\phi_0}\nabla\pi$ in the solvent.

Scalar activity was considered as precisely such a shift in pressure, where $^{\rm p}= s\kappa\ t)\nabla\delta\ \mathbf{r}\quad\mathbf{R})$. If we consider an isotropic distribution of either Types I or II active dipoles, such that $\langle\hat{\mathbf{n}}\hat{\mathbf{n}}\rangle=\frac{1}{3}I$, we obtain:

$$\langle\mathbf{f}\rangle = \quad\frac{af}{3}\kappa\ t)\nabla\delta\ \mathbf{r}\quad\mathbf{R})\tag{B41}$$

Thus, an isotropic solution of Type I dipoles simply increases (decreases) the osmotic pressure of polymer (solvent), and vice-versa for Type II dipoles. However, it is clearly physically unfeasible to place an infinite number of dipoles in a given location to produce such a local shift in osmotic pressure, so we must emphasize that this connection is purely formal.

ppendix C Transverse parts of singular flows

In solving for the transverse parts of the flows in the main text, we used the notation $^{\rm p}_{\perp}$, $^{\rm s}_{\perp}$ to indicate that we were applying the transverse projection operator to the sources in our equations of motion. Since these sources take the form of δ-functions or their gradients, the resulting objects may be ill-defined. Here, we show a procedure for handling them in the case of our equations of motion.

Our equations of motion are linear, and we consider them in an unbounded space. Thus, we may solve them via Fourier transform in space and time, which transforms the differential equations into algebraic equations. The transverse projection operator in Fourier space is

$$\mathscr{P}_{\ \beta} = \delta_{\ \beta}\quad\frac{q\ q_\beta}{q^2}\tag{C42}$$

for a wavevector $\mathbf{q}$, where $q=|\mathbf{q}|$. In general, we may consider a transverse velocity field $\mathbf{v}_\perp$ which obeys the following linear response relation

$$v_{\perp\ \mathbf{q}} = \mathscr{R}_{\ \beta\mathbf{q}} f_{\beta\mathbf{q}}\,,\tag{C43}$$

where all repeated indices except for $\mathbf{q}$ are summed over. Conveniently, in our case the response functions are diagonal in Fourier space, so all the tensorial structure is given by $\mathscr{P}$: $\mathscr{R}_{\ \beta\mathbf{q}} = g_q\mathscr{P}_{\ \beta\mathbf{q}}$, which simplifies the linear response relation

$$v_{\perp\ \mathbf{q}} = g_q\mathscr{P}_{\ \beta\mathbf{q}} f_{\beta\mathbf{q}}\tag{C44}$$

We define the real space Green's function of this system as follows:

$$v\quad\mathbf{r}) = \mathscr{R}_{\ \beta}\ \mathbf{r})f_\beta\ \mathbf{r})\tag{C45}$$

There are only two rank-2 tensors available to us, so we can write $\mathscr{R}$ as their linear combination:

$$\mathscr{R}_{\beta}(\mathbf{r}) = {}_{\mathscr{R}}(r)\delta_{\beta} + B_{\mathscr{R}}(r)\frac{r\, r_{\beta}}{r^2}, \tag{C46}$$

where ${}_{\mathscr{R}}$, $B_{\mathscr{R}}$ are some scalar functions of $r = |\mathbf{r}|$. To find these functions, we consider the following two invariant combinations:

$$\begin{aligned} \mathscr{R}_{\beta}\delta_{\beta} &= 3\,{}_{\mathscr{R}} + B_{\mathscr{R}} \\ \mathscr{R}_{\beta}\frac{r\, r_{\beta}}{r^2} &= {}_{\mathscr{R}} + r^2 B_{\mathscr{R}} \end{aligned} \tag{C47}$$

These scalar expressions can be further compared to their analogs in Fourier space:

$$\begin{aligned} \mathscr{R}_{\beta\mathbf{q}}\delta_{\beta} &= 2g_q \\ \mathscr{R}_{\beta\mathbf{q}}\frac{r\, r_{\beta}}{r^2} &= g_q\,(1 \quad \mathbf{q}\cdot\mathbf{r})) \end{aligned} \tag{C48}$$

It is then straightforward to take the inverse Fourier transform of expressions (C48) and compare them to the expressions (C47), and solve the resulting set of equations for ${}_{\mathscr{R}}, B_{\mathscr{R}}$.

These results can be checked by an alternate solution method, which is more reminiscent of traditional incompressible low-Reynolds number hydrodynamics. In that case, we implicitly take the transverse component of a velocity field by imposing incompressibility through an auxiliary scalar field, the pressure. The Stokes equations are:

$$\begin{aligned} \eta\nabla^2\mathbf{v} + \nabla P &= \mathbf{f} \\ \nabla\cdot\mathbf{v} &= 0 \end{aligned} \tag{C49}$$

and their solution is the well-known Oseen tensor[27]. We can take a similar strategy by taking our original equation of motion, foregoing the transverse projection operator on the force, and simply imposing incompressibility by adding an auxiliary pressure and a new equation: $\nabla\cdot\mathbf{v} = 0$. Using this technique gives the same results as the procedure outlined above.

ppendix D Estimates

Appendix D.1 RNA polymerase II as a source of activity

There are approximately 10^5 RNA polymerase II molecules in a HeLa cell[43], whose nucleus is approximately 10 μm across, leading to a density around 10^2 molecules/μm^3. The force exerted by RNA polymerase II is on the order of 10 pN, ranging up to 40 pN[25,44], and their step size is half a base-pair, corresponding to 0 16 nm[45]. The rate constants controlling the stepping process when it is not paused lie around 20 100 s ^{1}, meaning the step time is at a maximum around 0 05 s per step.

If we take the force density of these motors F_m, and multiply it by a step time $\tau_m \approx 0\,05$ s as well as a step size $d_m = 0\,016$ nm, we get a quantity with units of viscosity, which can be compared to the viscosity of the polymer, which is still poorly constrained in the case of chromatin but is likely in the range $\eta^{\mathrm{p}} \approx 0\,6$ 3000 Pas[34–39].

In this case we have $F_m\tau_m d_m \approx 0\,03$ Pa s, and therefore $F_m\tau_m d_m \ll \eta^{\mathrm{p}}$, so we don't expect a single RNA polymerase II event to generate a strain of order unity in chromatin.

To approximate the power spectrum magnitude in this case, if we take the size of a molecular motor to be 10 nm, its density 10^2 molecules/μm^3, and the viscosity of chromatin to be 1 Pas, then we get $\left(\frac{af}{\eta^{\mathrm{p}}}\right)^2\rho \simeq 1\mu\mathrm{m}^3 s^{\ 2}$.

Appendix D.2 Length scales of nonlocal rheology

Nonlocal effects are relevant for length scales r where $t/\tau_0) \gg \frac{r^4}{b^4}\tau_0$, where τ_0 is the Rouse relaxation time of a Kuhn length of polymer, and b is that Kuhn length (as shown in[26] Figure 3). In our case, $b \sim 100$ nm[30], and $\tau_0 = \frac{\eta^{\mathrm{s}} b^3}{T} \sim 10^{\ 4}$ s (estimated using viscosity of water and room temperature), where we measure temperature in units of energy, setting $k_B = 1$.

Notes and references

1 B. Alberts, A. Johnson, J. Lewis, D. Morgan, M. Raff, K. Roberts and P. Walter, *Molecular Biology of the Cell*, W.W. Norton, 2017.

2 R. Milo and R. Phillips, *Cell Biology By The Numbers*, Garland Science, 2015.

3 K. E. Van Holde, *Chromatin*, Springer Science & Business Media, 2012.

4 M. R. Hübner and D. L. Spector, *Annu. Rev. Biophys.*, 2010, **39**, 471–489.

5 A. Zidovska, *Curr. Opin. Genet. Dev.*, 2020, **61**, 83–90.

6 I. Bronstein, Y. Israel, E. Kepten, S. Mai, Y. Shav-Tal, E. Barkai and Y. Garini, *Phys. Rev. Lett.*, 2009, **103**, 018102.

7 V. Levi, Q. Ruan, M. Plutz, A. S. Belmont and E. Gratton, *Biophys. J.*, 2005, **89**, 4275–4285.

8 B. Chen, L. A. Gilbert, B. A. Cimini, J. Schnitzbauer, W. Zhang, G.-W. Li, J. Park, E. H. Blackburn, J. S. Weissman, L. S. Qi *et al.*, *Cell*, 2013, **155**, 1479–1491.

9 C.-H. Chuang, A. E. Carpenter, B. Fuchsova, T. Johnson, P. de Lanerolle and A. S. Belmont, *Curr. Biol.*, 2006, **16**, 825–831.

10 A. Zidovska, D. A. Weitz and T. J. Mitchison, *Proc. Natl. Acad. Sci. USA*, 2013, **110**, 15555–15560.

11 D. Saintillan, M. J. Shelley and A. Zidovska, *Proc. Natl. Acad. Sci. USA*, 2018, **115**, 11442–11447.

12 R. Bruinsma, A. Y. Grosberg, Y. Rabin and A. Zidovska, *Biophys. J.*, 2014, **106**, 1871–1881.

13 E. Lieberman-Aiden, N. L. Van Berkum, L. Williams, M. Imakaev, T. Ragoczy, A. Telling, I. Amit, B. R. Lajoie, P. J. Sabo, M. O. Dorschner *et al.*, *Science*, 2009, **326**, 289–293.

14 H. Kang, Y.-G. Yoon, D. Thirumalai and C. Hyeon, *Phys. Rev. Lett.*, 2015, **115**, 198102.

15 L. Liu, G. Shi, D. Thirumalai and C. Hyeon, *PLoS Comput. Biol.*, 2018, **14**, e1006617.

16 G. Shi, L. Liu, C. Hyeon and D. Thirumalai, *Nat. Commun.*, 2018, **9**, 1–13.

17 M. Di Pierro, B. Zhang, E. L. Aiden, P. G. Wolynes and J. N. Onuchic, *Proc. Natl. Acad. Sci. USA*, 2016, **113**, 12168–12173.

18 T. Sakaue and T. Saito, *Soft Matter*, 2017, **13**, 81–87.

19 A. Grosberg, Y. Rabin, S. Havlin and A. Neer, *EPL Europhys. Lett.)*, 1993, **23**, 373.

20 M. V. Tamm, L. I. Nazarov, A. A. Gavrilov and A. V. Chertovich, *Phys. Rev. Lett.*, 2015, **114**, 178102.

21 D. Michieletto, E. Orlandini and D. Marenduzzo, *Phys. Rev. X*, 2016, **6**, 041047.

22 R. Laghmach, M. Di Pierro and D. A. Potoyan, *Biophys. J.*, 2020, **118**, 2130–2140.

23 M. Di Pierro, D. A. Potoyan, P. G. Wolynes and J. N. Onuchic, *Proc. Natl. Acad. Sci. USA*, 2018, **115**, 7753–7758.

24 M. Doi and A. Onuki, *J. Phys. II*, 1992, **2**, 1631–1656.

25 H. Yin, M. D. Wang, K. Svoboda, R. Landick, S. M. Block and J. Gelles, *Science*, 1995, **270**, 1653–1657.

26 Y. Rabin and A. Y. Grosberg, *Macromolecules*, 2019, **52**, 6927–6934.

27 M. Doi and S. F. Edwards, *The Theory of Polymer Dynamics*, Oxford University Press, 1988.

28 S. Adelman, *J. Chem. Phys.*, 1978, **68**, 49–55.

29 S. M. Görisch, K. Richter, M. O. Scheuermann, H. Herrmann and P. Lichter, *Exp. Cell Res.*, 2003, **289**, 282–294.

30 I. Solovei, A. Cavallo, L. Schermelleh, F. Jaunin, C. Scasselati, D. Cmarko, C. Cremer, S. Fakan and T. Cremer, *Exp. Cell Res.*, 2002, **276**, 10–23.

31 S. Kühner, V. van Noort, M. J. Betts, A. Leo-Macias, C. Batisse, M. Rode, T. Yamada, T. Maier, S. Bader, P. Beltran-Alvarez *et al.*, *Science*, 2009, **326**, 1235–1240.

32 L. Liang, X. Wang, X. Da, T. Chen and W. R. Chen, *J. Biomed. Opt.*, 2009, **14**, 024013.

33 F. Erdel, M. Baum and K. Rippe, *J. Phys - Condens. Mat.*, 2015, **27**, 064115.

34 Y. Tseng, J. S. Lee, T. P. Kole, I. Jiang and D. Wirtz, *J. Cell Sci.*, 2004, **117**, 2159–2167.

35 F. M. Hameed, M. Rao and G. Shivashankar, *PLoS One*, 2012, **7**, e45843.

36 A. Celedon, C. M. Hale and D. Wirtz, *Biophys. J.*, 2011, **101**, 1880–1886.

37 A. H. de Vries, B. E. Krenn, R. van Driel, V. Subramaniam and J. S. Kanger, *Nano Lett.*, 2007, **7**, 1424–1427.

38 I. Eshghi, J. A. Eaton and A. Zidovska, *Phys. Rev. Lett.*, 2021, **126**, 228101.

39 C. M. Caragine, S. C. Haley and A. Zidovska, *Phys. Rev. Lett.*, 2018, **121**, 148101.

40 A. Zidovska, *Biophys. Rev.*, 2020, **12**, 1093–1106.

41 D. L. Lafontaine, J. A. Riback, R. Bascetin and C. P. Brangwynne, *Nat. Rev. Mol. Cell Bio.*, 2021, **22**, 165–182.

42 L. Durlofsky and J. Brady, *Phys. Fluids*, 1987, **30**, 3329–3341.

43 H. Kimura, Y. Tao, R. G. Roeder and P. R. Cook, *Mol. Cell Biol.*, 1999, **19**, 5383–5392.

44 E. A. Galburt, S. W. Grill, A. Wiedmann, L. Lubkowska, J. Choy, E. Nogales, M. Kashlev and C. Bustamante, *Nature*, 2007, **446**, 820–823.

45 M. Dangkulwanich, T. Ishibashi, S. Liu, M. L. Kireeva, L. Lubkowska, M. Kashlev and C. J. Bustamante, *Elife*, 2013, **2**, e00971.